Study of Light Transport in Diffuse Media

A thesis submitted towards partial fulfillment of
BS-MS Dual Degree Programme

by
Harshavardhan Ashok Gaonkar

under the guidance of

Dr. Ramasubramaniam Rajagopal
Senior Research Scientist, Unilever R & D, Bangalore

Indian Institute of Science Education and Research Pune

Certificate

This is to certify that this thesis entitled "**Study of Light Transport in Diffuse Media**" submitted towards the partial fulfillment of the BS-MS dual degree programme at the Indian Institute of Science Education and Research Pune represents original research carried out by Harshavardhan Ashok Gaonkar at Unilever R & D, Bangalore, under the supervision of Dr.Ramasubramaniam Rajagopal during the academic year 2012-2013.

Harshavardhan Ashok Gaonkar Dr.Ramasubramaniam Rajagopal

Acknowledgements

I would like to offer my profoundest gratitude to my thesis advisor, Dr. Ram Rajagopal. From helping me understand the basics of light transport to the process of writing the thesis, Dr.Ram has offered his unreserved help and guidance. It would have been impossible to achieve this goal without his constant support, encouragement and also his joking jabs at my incompetence. I consider myself to be fortunate to be associated with him who has given a decisive turn to my career.

I would also like to thank Arindam Roy, who was involved in this project from the start and was a great help in running the experiments. His support and positive inputs have been invaluable.

I would not have contemplated this road if not for my parents, who instilled within me a love of creative pursuits, science and research, all of which finds a place in this thesis. To my parents, thank you.

Abstract

In materials where both absorption and scattering are present, measurement of absorption becomes difficult since it is not possible to decouple absorption from scattering using standard absorption spectroscopy techniques. Various authors have tried to use diffuse optical spectroscopy to address this. However these measurements involve computer intensive calculations to obtain optical parameters from the diffuse optical spectra. Kubelka-Munk (K-M) theory is a phenomenological light transport theory that provides analytical expressions for reflectance and transmittance of diffusive substrates. Many authors have derived relations between coefficients of K-M theory and that of the more fundamental radiative transfer equations (RTE). These relations are valid only in the diffusive light transport regime where scattering dominates over absorption. They also fail near boundaries where incident beams are not diffusive.

In this thesis, we have developed an integrating sphere based diffuse optical measurement system. Using the system, we measured total transmittance and total reflectance of samples with varying optical parameters and obtained empirical relations between K-M coefficients and the radiative transport coefficients which are valid both in the diffusive and non-diffusive regimes. Our empirical relations show that the K-M scattering coefficients depend only on reduced scattering coefficient (μ_s') while the K-M absorption coefficient depends both on absorption (μ_a) and reduced scattering (μ_s') coefficients of radiative transfer theory. We have shown that these empirical relations can predict total reflectance within an error of 10%. They also can be used to solve the inverse problem of obtaining multiple optical parameters such as chromophores concentration and sample thickness from the measured reflectance spectra with a maximum accuracy of 90-95%.

We have also used our method to decouple the absorption and scattering properties of micron sized iron oxide particles which is not possible with standard absorption spectroscopy techniques. Our method is capable of measuring the specific absorption of iron oxide within 5-10% error. This method along with the derived empirical relations can be further extended to UV regimes to study nanoparticles which are of relevance in various photonic applications.

List of Figures

Figure 1: Illustration of light transport in an optical medium modelled using the Kubelka-Munk theory. *I* and *J* depict diffuse fluxes traveling in the forward and backward directions, respectively. *S* and *K* are the backscattering and absorption coefficients

Figure 2: Schematic for the experimental procedure followed to arrive at the empirical relation

Figure 3. Absorption spectra of the dye used. (a) Chocolate Brown TAS dye. (b) Premium Dark Chocolate dye

Figure 4. Schematic of the single wavelength measurements. (a) Reflectance and (b) Transmittance

Figure 5: Single port measurements. (a) Reference measurement and (b) sample measurement

Figure 6: Dual port measurement system for decreasing measurement errors. (a) Reference Measurement (b) Sample Measurement

Figure 7: Custom built full spectrum transmittance system

Figure 8: Measured values of (a) total transmittance and (b) total reflectance of samples for various values of μa and μs' at 488nm

Figure 9: (a) K-M scattering coefficient *S* and (b) K-M absorption coefficient *K* for samples with various values of μ_a and μ_s'.*K* and *S* were obtained from the measured total reflectance (*R*) and total transmittance (*T*)

Figure 10: Predicted values of *S* and *K* using the empirical relations in Eqs. (4.1) and (4.2) as a function of *S* and *K* values calculated from measured *R* and *T* using Eq. (1.11)

Figure 11: Measured and predicted reflectance spectra for 5 different samples (a) Reflectance values; (b) Error in predicted reflectance

Figure 12: Solving for optical parameters from the measured reflectance spectra of samples. The best fits were obtained by varying two fitting parameters, namely dye concentration and layer thickness. The symbols show measured reflectance, and solid lines show the best fit from the model. The actual parameter values and the predicted values are shown in Table 3

Figure 13: Iron Oxide particles dispersed in pentacyclo-siloxane oil

Figure 14: Measured values of absorbance of iron oxide dispersion and Allura red dye measured using a standard UV-Vis absorption spectrometer.

Figure 15: Measured values of (a) total reflectance (R) and (b) total transmittance (T) of 4 different concentrations of iron oxide dispersion over 450-650 nm range.

Figure 16: (a) Absorption coefficient and (b) scattering coefficient for the 4 concentrations of iron oxide dispersions. μ_a and μ_s' were obtained using equations (4.1) and (4.2) from the measured total reflectance(R) and total transmittance (T) in Figure 15

Figure 17: Specific absorption coefficient of iron oxide particles. Error bars indicate standard deviation of four different concentrations

Contents

1.INTRODUCTION: LIGHT TRANSPORT IN SCATTERING MEDIA 1

1.1 Absorption 1
1.2 Light Scattering 2
1.3 Scattering Theories 3
1.4 Absorption in the Presence of Scattering 4

1.4 .1 Radiative Transport Equation 4
1.4.2 RTE in diffuse media 5
1.4.3 Kubelka-Munk Theory 6

2.DEVELOPMENT OF RELATION BETWEEN KUBELKA –MUNK AND RADIATIVE TRANSFER COEFFICIENTS 8

3.MATERIALS AND METHODS 11

3.1 Sample Preparation 11
3.2 Development of the diffuse optical measurement system 12

3.2.1 Single wavelength measurements 12
3.2.2 Single port measurements 13
3.2.3 Dual port measurements 14
3.2.4 Full spectrum reflectance and transmittance measurements 15

4.RESULTS AND DISCUSSIONS 17

4.1 Empirical relations between K-M and radiative transfer coefficients 17

4.1.1 Measurement of total reflectance and transmittance 17
4.1.2 Calculation of K-M coefficients *K* and *S* 17
4.1.3 Empirical relation between K-M and Radiative transfer coefficients 19
4.1.4 Validation of Empirical Relations 21

4.2 Applications 23

4.2.1 Extracting optical parameters from measured reflectance 23
4.2.2 Measurement of absorption coefficient of highly scattering particles 24

5.CONCLUSION 30

REFERENCES 31
APPENDIX 33

Chapter 1

INTRODUCTION: LIGHT TRANSPORT IN SCATTERING MEDIA

When light enters any media, it undergoes various physical processes such as absorption, scattering etc. This chapter describes these mechanisms that govern light transport and interaction through an optical medium. Section 1.1 describes the concept of light absorption introducing laws and definitions relevant to its quantification and measurement. In Section 1.2 the basic theory behind light scattering and the parameters used to define it are introduced. The discussion is limited to elastic scattering, in which there is no loss in energy of the scattered light. Section 1.3 discusses the Mie theory of scattering and the Rayleigh approximation. Section 1.4 describes the case of absorption in the presence of scattering and the theories that are used to understand such systems viz. the Radiative Transport Equation and the Kubelka-Munk Theory

1.1 Absorption

When radiation is incident on a material, the discrete charges present in the material are forced to oscillate at the frequency of the incident electric field. When the frequency of the incident light is comparable to the natural frequencies at which atoms or molecules vibrate in the absence of an applied field, resonance will occur around the natural frequencies, whereby energy is transferred from the incident field to the system and its amplitude of vibration is greatly increased. These excited atoms seldom get a chance to lose this energy through radiative processes, mechanical collisions with their neighboring atoms happens much faster raising the kinetic energy of the other particles involved in the collisions. Hence, the energy associated with the incident field is most often dissipated as heat within the medium. This process is known as absorption. The overall effect of absorption is a reduction in the intensity of the light beam traversing the medium.

In 1729, the French mathematician Pierre Bouguer obtained a relationship between the absorption of light in a purely absorbing medium and the thickness of the medium[1].This was formalized into a mathematical expression by Johann Lambert, now known as the Lambert-Bouguer Law

$$\frac{dI}{I} = \mu_a dl \tag{1.1}$$

which describes how each successive layer d*l* of the medium absorbs the same fraction $\frac{dI}{I}$ of the incident intensity I for a constant μ_a, the absorption coefficient. For incident intensity I_0, therefore, the transmitted intensity I through a distance l will be

$$I = I_0\, exp(-\mu_a . l) \tag{1.2}$$

The absorption coefficient μ_a can be interpreted as the probability that a photon will be absorbed by the medium per unit length. The reciprocal of the absorption coefficient, known as the absorption length, is the distance required for the intensity of the beam to fall to *1/e* of the initial intensity. This relationship was further extended by August Beer who related the absorption coefficient linearly to its concentration 'c' [2]

$$\mu_a = \alpha . c \tag{1.3}$$

where α is known as the specific absorption coefficient. Substituting for μ_a in the Lambert Bouguer law(Eqn 1.2) gives what is known as the Beer-Lambert law

$$I = I_0\, exp(-\alpha . c . l) \tag{1.4}$$

There are certain limiting conditions where the Beer-Lambert law works: firstly the light entering the medium must be perfectly collimated, and the medium itself must be completely homogenous.

1.2 Light Scattering

When charged particles in a medium are set into oscillatory motion by the electric field of the incident wave, and re-emit (as opposed to absorb) light of the same frequency as the primary wave, the process is called scattering. Scattering intensities are much weaker than absorption, as scattering occurs at non-resonance frequencies, since the forced vibrational amplitudes of the particles are much smaller than those at natural resonances.

The scattering cross-section, $\sigma_{s,}$ is often used when studying scattering. It describes the ability of a particle to scatter light and is expressed as the effective surface area that a perfectly absorbing disk would have in order to produce the same attenuation of a collimated beam, measured by a collimated detector, as the scattering particle. The scattering coefficient and the scattering cross-section are related as follows

$$\mu_s = \rho.\sigma_s \tag{1.5}$$

where ρ is the particle number density in the medium.

1.3 Scattering Theories

Mie solution to Maxwell's equations (also known as the Lorenz–Mie solution or Mie scattering) describes the scattering of electromagnetic radiation by a sphere. Mie's scattering model can be used to find the radial and angular distribution of intensity of the scattered radiation. The intensity of Mie scattered radiation is given by the summation of an infinite series which can be numerically calculated. It is named after Gustav Mie.

Rayleigh scattering describes the elastic scattering of light by spheres which are much smaller than the wavelength of light. The intensity (I) of the scattered radiation is given by

$$I = I_0 \frac{8\pi^4 N\alpha^2}{\lambda^4 R^2}(1+\cos^2\theta) \tag{1.6}$$

where I_0 is the light intensity before the interaction with the particle, N is the number of scattering particles, R is the distance between the particle and the observer, θ is the scattering angle, λ the wavelength of the incident light and α is the polarizability [3]. It can be seen from the above equation that Rayleigh scattering is strongly dependent upon the wavelength of the incident light. Furthermore, the intensity of Rayleigh scattered radiation is identical in the forward and reverse directions.

The Rayleigh scattering model breaks down when the particle size becomes larger than around 10% of the wavelength of the incident radiation. In the case of particles with dimensions greater than this, Mie's solutions can be used. Mie scattering differs from Rayleigh scattering in several

respects; it is roughly independent of wavelength and it is larger in the forward direction than in the reverse direction. The greater the particle size, the more of the light is scattered in the forward direction. [4,5]

Complete solutions to Mie scattering are known only for well-defined spherical shaped and uniformly sized particles. Scattering systems with irregular particles can only be understood using complex mathematical models and computer simulations

1.4 Absorption in the Presence of Scattering

A wide variety of real-world systems exhibit both absorption and scattering phenomena. The light that enters such media can undergo multiple scattering events before being absorbed by the media [6]. Light transport becomes randomized and does not travel in a straight line. Due to this randomization of light paths, quantification of absorption losses using Beer-Lambert's Law (Eqn 1.4) is no longer possible. To study such systems we need to look at other theories and models which work well with absorption and scattering simultaneously. One such theory is the radiative transport equation.

1.4 .1 Radiative Transport Equation

Radiative transport equation (RTE) treats light as a form of radiation energy and models how the energy flows and interacts with the media. Consider a small packet of light energy L, defined by its position r and its direction of propagation $\hat{s}$, called the spectral radiance which acts as the fundamental quantity in RTE. The radiance $L(r,\hat{s})$ can be lost either by absorption or scattering. But it also can be gained from the light scattered into its direction from other directions $\hat{s}'$. These two processes are captured by the radiative transport equation;

$$\hat{s}.\nabla L(r,\hat{s}) = -(\mu_a + \mu_s)L(r,\hat{s}) + \frac{\mu_s}{4\pi}\int p(\hat{s},\hat{s}')d\Omega \tag{1.7}$$

Here the integral is over all solid angles and $d\Omega$ is the differential solid angle in the direction$\hat{s}$. μ_a, μ_s' are the absorption and scattering coefficients of the media also known as the radiative transport coefficients. $p(\hat{s},\hat{s}')$ is the scattering phase function and it is defined as the probability

that photons travelling in the direction $\hat{s}$ are scattered into the $\hat{s}'$ direction[7,8]. The scattering phase function is normalized as $\int p(\hat{s},\hat{s}')d\Omega = 1$ over all angles.

RTE ignores wave amplitudes and phases and hence cannot describe wave phenomena like diffraction or interference. Formulation of the transport equation assumes that each scattering particle is sufficiently distant from its neighbors to prevent interactions between successive scattering effects. In theory, these scatterers and absorbers must be uniformly distributed throughout the medium. Calculations of light distribution based on the radiative transport equation require knowledge of the absorption and scattering coefficients, and the phase function. Yet, to arrive at these parameters, one must first have a solution of the radiative transport equation. Because of the difficulty of solving the transport equation exactly, several approximations are generally used.

1.4.2 RTE in diffuse media

Scattering by a single localized scattering center is called single scattering. However in real-world systems the scattering centers are usually grouped together and the radiation is scattered more than once. This is called multiple scattering. Multiple scattering events cause the incoming radiation to be directionally randomized on interaction with the media. This light which has lost its initial directional properties due to multiple scattering events is called diffuse light. In the diffusive transport regime where scattering dominates over absorption ($\mu_s >> \mu_a$)the light photon undergoes multiple scattering events before either being absorbed or exiting the media.

By the nature of RTE, every single absorption and scattering event that takes place in the media is considered in the equation (Eqn 1.7). In diffuse media where a photon will undergo multiple scattering events before being absorbed or exiting the media, it becomes very tedious and complex to understand each of the interactions. Although the RTE (Eqn 1.7) is theoretically complete, extracting meaningful solutions in such diffuse systems becomes computationally very intensive due to anisotropic multiple scattering events. To simplify this, these multiple scattering events are captured by the reduced scattering coefficient μ_s' which is the inverse of the path length required for the complete randomization of the photon direction and is defined as

$$\mu_s' = \mu_s(1-g) \tag{1.8}$$

where g is the anisotropy factor defined as

$$g = \int p(\theta)\cos(\theta)d\hat{s}' \tag{1.9}$$

g takes value from -1 to +1. If the scattering is completely isotropic g will be equal to zero as p is equal for all angles. As the particle size increases, however, the intensity distribution increases in the forward direction and p for small angles is much higher than for all other angles. Therefore, the mean cosine tends towards a value of unity, the higher the g value the more forward-peaked the scattering.

1.4.3 Kubelka-Munk Theory

Another approach to studying light transport in highly scattering media is the phenomenological Kubelka-Munk(K-M) theory. K-M theory assumes a media which is completely homogenous, a plane layer of finite thickness but infinite width and length, which is illuminated by a perfectly diffuse and homogenous source of light. The radiation passing through the medium can be divided into two "diffuse fluxes" traveling in the forward and backward directions denoted as *I*

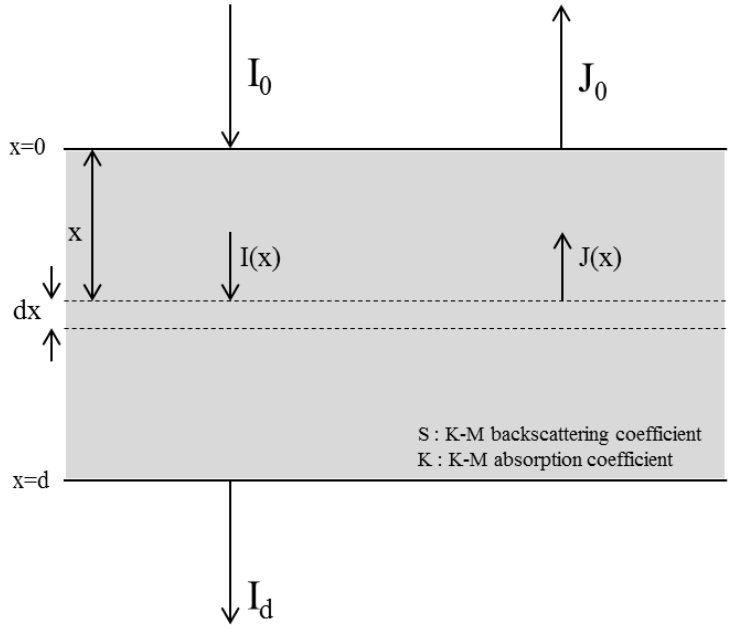

Figure 1: Illustration of light transport in an optical medium modeled using the Kubelka-Munk theory. *I* and *J* depict diffuse fluxes traveling in the forward and backward directions, respectively. *S* and *K* are the backscattering and absorption coefficients

and *J*, respectively (see Figure 1). The K-M backscattering and absorption coefficients for these diffuse fluxes (denoted as S and K, respectively) are defined by two differential equations:

$$\begin{aligned} I(x+dx) &= (K+S).I + S.J + I(x) \\ J(x) &= -(K+S).J + S.I + J(x+dx) \end{aligned} \tag{1.10}$$

On integrating these equations over the complete thickness *d* of the media and applying boundary conditions [9], we obtain

$$\begin{aligned} R &= \frac{\left(1-\beta^2\right)\left(\exp\left(\alpha d\right)-\exp\left(-\alpha d\right)\right)}{\left(1+\beta\right)^2\exp\left(\alpha d\right)-\left(1-\beta\right)^2\exp\left(-\alpha d\right)} \\ T &= \frac{4\beta}{\left(1+\beta\right)^2\exp\left(\alpha d\right)-\left(1-\beta\right)^2\exp\left(-\alpha d\right)} \\ \alpha &= \sqrt{K\left(K+2S\right)},\ \beta = \sqrt{\frac{K}{K+2S}} \end{aligned} \tag{1.11}$$

The KM equations relate the absorption and scattering properties of the media to its reflectance and transmittance. Due to its simplicity in computation, KM theory is widely used in many applications.

Chapter 2

DEVELOPMENT OF RELATION BETWEEN KUBELKA –MUNK AND RADIATIVE TRANSFER COEFFICIENTS

The Kubelka-Munk (K-M) equations are very powerful tools in extracting the absorption and scattering properties of the media using easily available transmittance and reflectance data. However the K-M coefficients are only phenomenological approximations because the theory assumes incident radiation is diffuse and that the scattering is isotropic. Similar to other diffusion approximation based models, K-M theory also assumes higher scattering compared to absorption. Though these conditions are not completely met in many of the real systems, the theory nonetheless provides a simple quantitative way of describing light transport in diffused medium. Many authors [10-13] have derived relations between the K-M coefficients and the more fundamental radiative transfer coefficients (μ_a, μ_s and g) as defined in chapter 1. In the diffusive approximation regime, where ($\mu_s >> \mu_a$), the general form of the relations between the K-M coefficients and the radiative transfer coefficients derived by different authors can be written as

$$\begin{aligned} S &= x\mu_s^{'} - y\mu_a \\ K &= z\mu_a \end{aligned} \tag{2.1}$$

For an isotropic medium, Klier [10] had shown $\mu_a = \eta K$ and $\mu_s = \chi S$ with the value of η varying from 0.5 to 1 while the value of χ varying from 4/3 to 3.33. van Gemert and Star [11] extended this further to show that the K-M coefficients can be related to the reduced scattering coefficient in an anisotropic medium. For an anisotropic and highly scattering medium, they showed $K = 2\mu_a$ and $S = (3\mu_s(1-g) - \mu_a)/4$. However, in most of the measurement geometries, the condition that the incident beam is diffusive is not met. It is either fully collimated or partly collimated and partly diffusive.

Various authors have extended this model further to include collimated incident flux and have shown that the K-M theory is also applicable in the case of collimated beam [14-16]. Thennadil

[16] has shown that, for a collimated incident beam in the high scattering regime, *S* depends only on scattering, however the relation should be modified to include a function dependent on the anisotropy factor, $S=12\mu_s'/(4.8446+.472g-.114g^2)^2$. However, here again, the theory is valid only in the diffusive regime, where scattering dominates absorption.

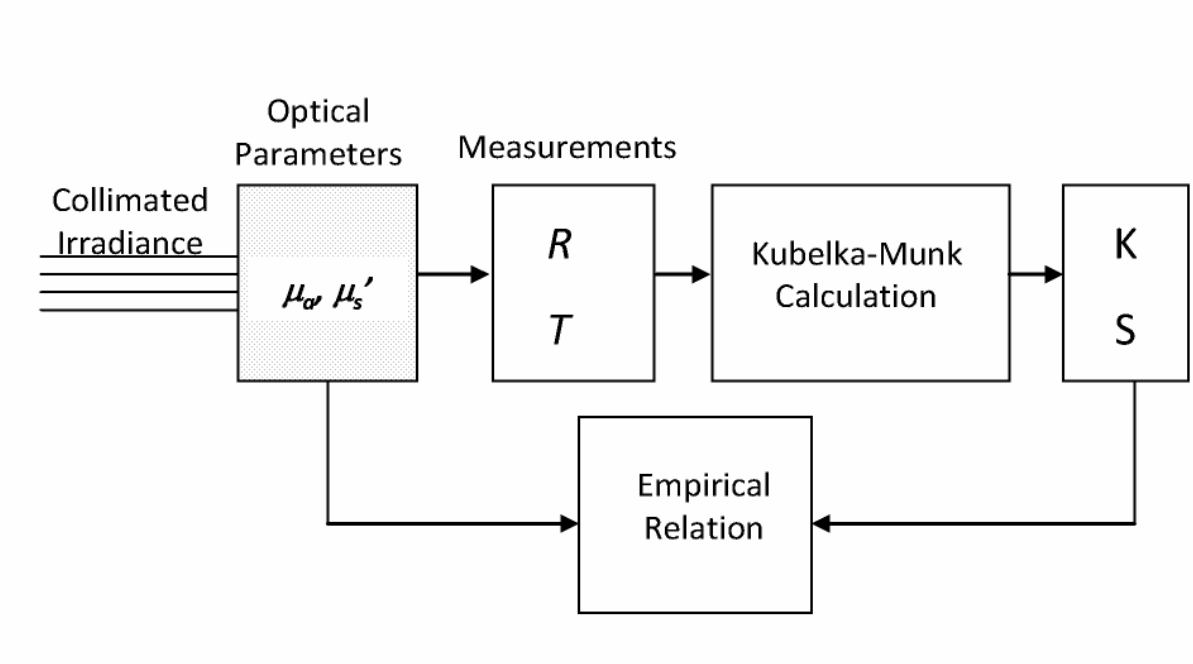

Figure 2: Schematic for the experimental procedure followed to arrive at the empirical relation

In most of the measurement systems, the incident beam is a broad collimated beam. While some of the theories mentioned above [14-16] have limitations due to various approximations involved, there are no existing relations between the K-M and radiative transfer coefficients both in the diffusive and non-diffusive regimes. In many systems, the diffusive regime is valid only in narrow range of wavelengths where scattering dominates absorption. For example in media which show a strong absorption in the blue region, the diffusion approximation based theories are not valid limiting the applicability of the theories. In this thesis, we wanted to develop an empirical relationship between the K-M and the radiative transfer coefficients for a broad collimated incident beam (standard in many measurement systems) which is valid for both diffusive ($\mu_a >> \mu_s'$) and non diffusive ($\mu_a < \mu_s'$) regime. The approach we have followed is schematically shown in Figure 2.

Samples with wide range of scattering and absorption properties (μ_a, μ_s') were prepared. The total transmittance (collimated and diffuse) *T* and total reflectance (specular and diffuse) *R* of the samples were measured. Using the values and *T* and *R*, equation 1.11 was solved to obtain corresponding K-M coefficient *K* and *S*. The empirical relations between the (*K*, *S*) and (μ_a, μ_s') were obtained. We have used this empirical relation to obtain optical parameters of scattering samples from measured reflectance spectrum. We have also used this relation to decouple the scattering and absorption properties of inorganic particles such as iron oxide which cannot be measured using standard absorption spectroscopy measurements.

Chapter 3

MATERIALS AND METHODS

3.1 Sample Preparation

Samples with different optical parameters were prepared in a 750 micron thick glass cuvette by dispersing known concentrations of polystyrene microspheres and one of the two brown colored dyes in milliQ water. The Premium Dark Chocolate dye was procured from Devarsons Industries Private Ltd, India and the Chocolate Brown TAS dyes was procured from Roha Dyechem Private Ltd, India. Polystyrene microspheres of 0.5 and 1 micron diameter were procured from Duke scientific, USA. Absorption coefficient of the dye and the scattering coefficient of the polystyrene spheres were measured using a Perkin Elmer Lamda900 UV-Vis spectrophotometer. The wavelength dependent absorption coefficients of the two dyes for 10 ppm concentration are shown in Figure 3.The anisotropy factor *g* was calculated using a web based Mie scattering calculator developed by Philip Laven [17]. The reduced scattering coefficients were calculated using Equation 1.8

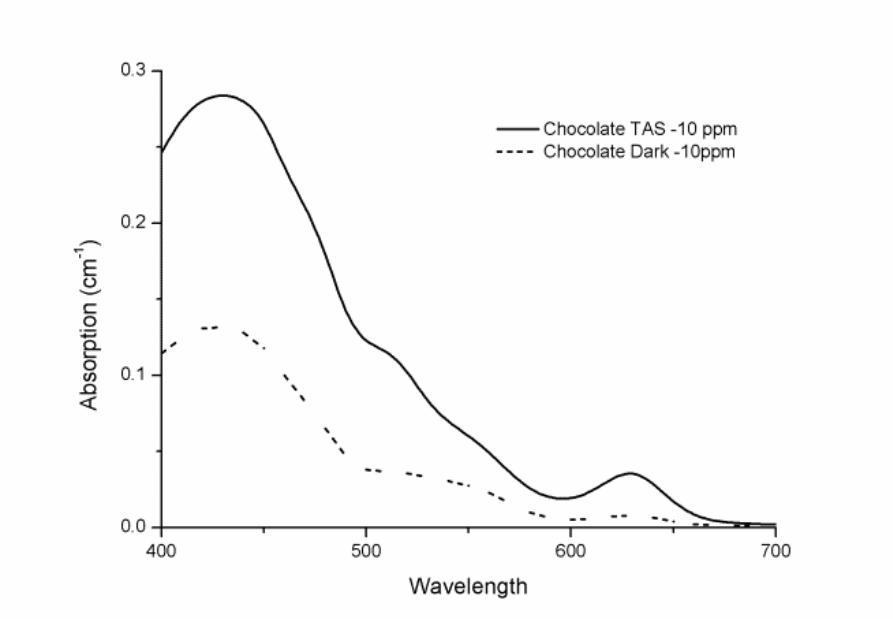

Figure 3. Absorption spectra of the dye used. (a) Chocolate Brown TAS dye. (b) Premium Dark Chocolate dye

3.2 Development of the diffuse optical measurement system

3.2.1 Single wavelength measurements

Total transmittance (collimated and diffused)*T* and total reflectance (specular and diffused)*R*, at 488nm, of the samples were measured using an Ar-ion laser (LEXEL, USA), a 90 mm diameter integrating sphere (Labsphere, USA) and a spectrometer (ILT 900 from International light, USA). The configurations used in these measurements are shown in Figure 4a and 4b.

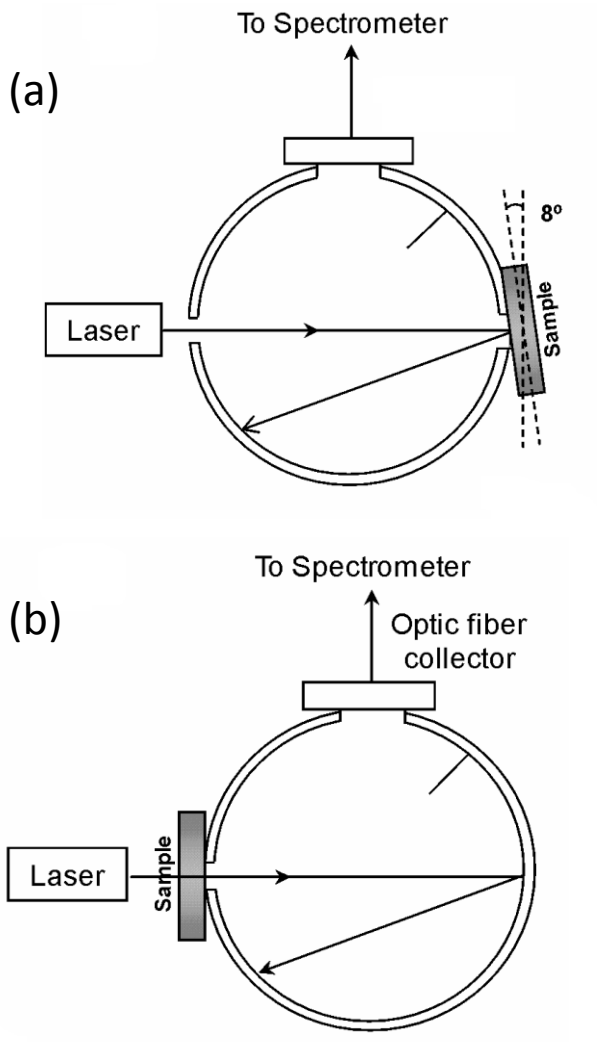

Figure 4. Schematic of the single wavelength measurements. (a) Reflectance and (b) Transmittance

Reflectance was measured relative to a Spectralon® reflectance standard with a reflectance value of 99% in the 400-650nm range. For reflectance measurement, the sample was held 8 degrees with respect to the direction of normal incidence in order to include the specular component of the reflected beam. The specular and the diffuse reflected light was collected by the integrating sphere and measured using the spectrometer. During total transmittance measurement, the transmitted light was collected by an integrating sphere and measured using a spectrometer.

A water filled cuvette was used as reference during transmittance measurements in order to account for reflectance losses from the cuvette walls. Reflectance from a water filled reference cuvette was subtracted from the measured reflectance in order to obtain reflectance from the sample alone.

3.2.2 Single port measurements

The transmittance and reflectance values of varying concentrations of purely scattering polystyrene beads were recorded at 488 nm. The values are shown in table 1. In the absence of any absorption, the sum of transmittance and reflectance values is expected to be 100%. However it was observed that the sum of T and R was consistently higher than 100% indicating inaccuracies in the measurements.

Table 1: Transmittance (T) and Reflectance (R) values for polystyrene beads using a single port measurement system

Sample	Transmittance (T)	Reflectance (R)	T+R
Concentration 1	82%	24%	106%
Concentration 2	76%	31%	107%
Concentration 3	73%	34%	107%

On closer scrutiny it was found that the differences in the reflective properties of our sample and reference cuvettes were leading to errors in the transmittance measurements. In the initial measurement of the water reference, the light is transmitted through the water samples, internally

reflected multiple times in the integrating sphere and a small fraction of the light is transmitted

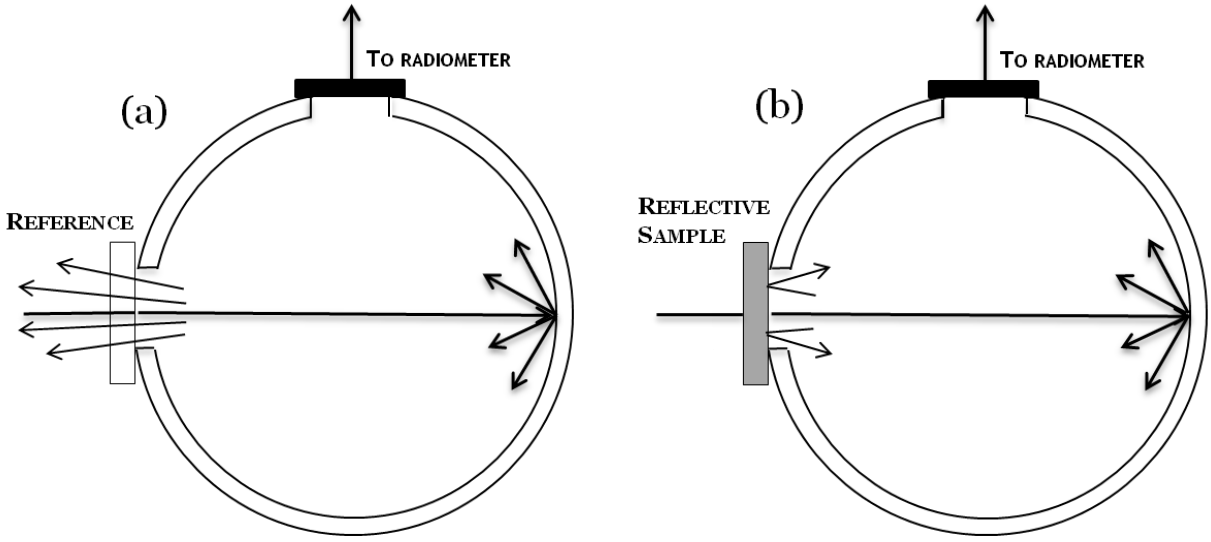

Figure 5: Single port measurements (a) Reference measurement and (b) sample measurement

back outside the sphere (see Figure 5a).However, in the case of the scattering sample, only a very small fraction of light is transmitted back from the inside of the integrating sphere and most of the light is reflected back (see Figure 5b) into the sphere itself. This causes a mismatch in the amount of light that is lost from the integrating sphere due to reflection in the two cases. A higher amount of light is collected in the sample measurement and thus the transmittance measurements are overestimated.

3.2.3 Dual port measurements

To rectify the single port measurement error, we used a dual port measurement system as shown in Figure 6.When taking the reference measurement, the reference cuvette was placed at the entry port and the sample cuvette was placed at the dummy port of the integrating sphere. In the sample measurement their positions were reversed. This ensures that the amount of light lost from the integrating sphere in both the measurements is nearly the same, resulting in minimization of measurement errors.

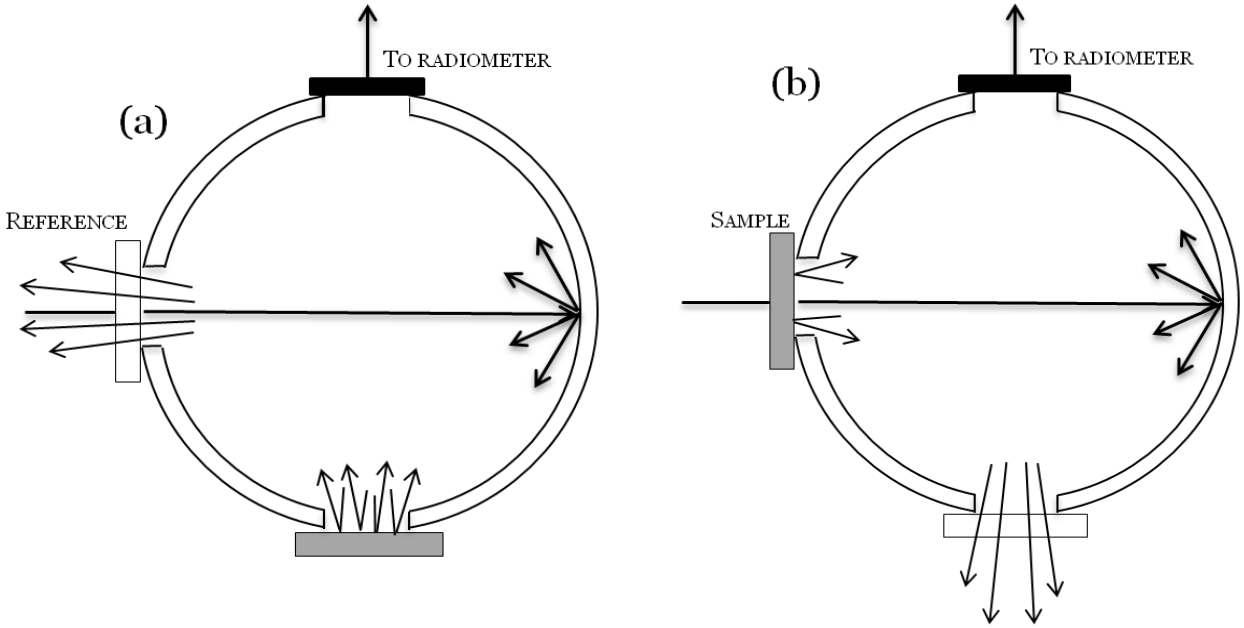

Figure 6: Dual port measurement system for decreasing measurement errors. (a) Reference Measurement (b) Sample Measurement

When the T and R of non absorbing samples with varying concentration were measured using the dual port method, we found that the errors in measurement were considerably reduced (Table2). The total of T and R values were close to 100%.

Table 2: The transmittance and reflectance values of purely scattering polystyrene samples in the dual port geometry

Sample	Transmittance (T)	Reflectance (R)	T+R
Concentration 1	75%	24%	99%
Concentration 2	69%	31%	99%
Concentration 3	66%	34%	100%

3.2.4 Full spectrum reflectance and transmittance measurements

The wavelength dependent reflectance spectra were measured using a handheld spectrophotometer (CM-2600d, Minolta, Japan). It is equipped with a Xenon light source and a 52 mm diameter integrating sphere. The sample was illuminated through an 8 mm diameter

aperture. The integrating sphere and the small aperture ensure that a broad collimated beam is incident on the sample. The reflected light is collected through the same aperture in the 8 degree viewing angle and is analyzed using a diffraction grating and a photodiode array. The reflectance

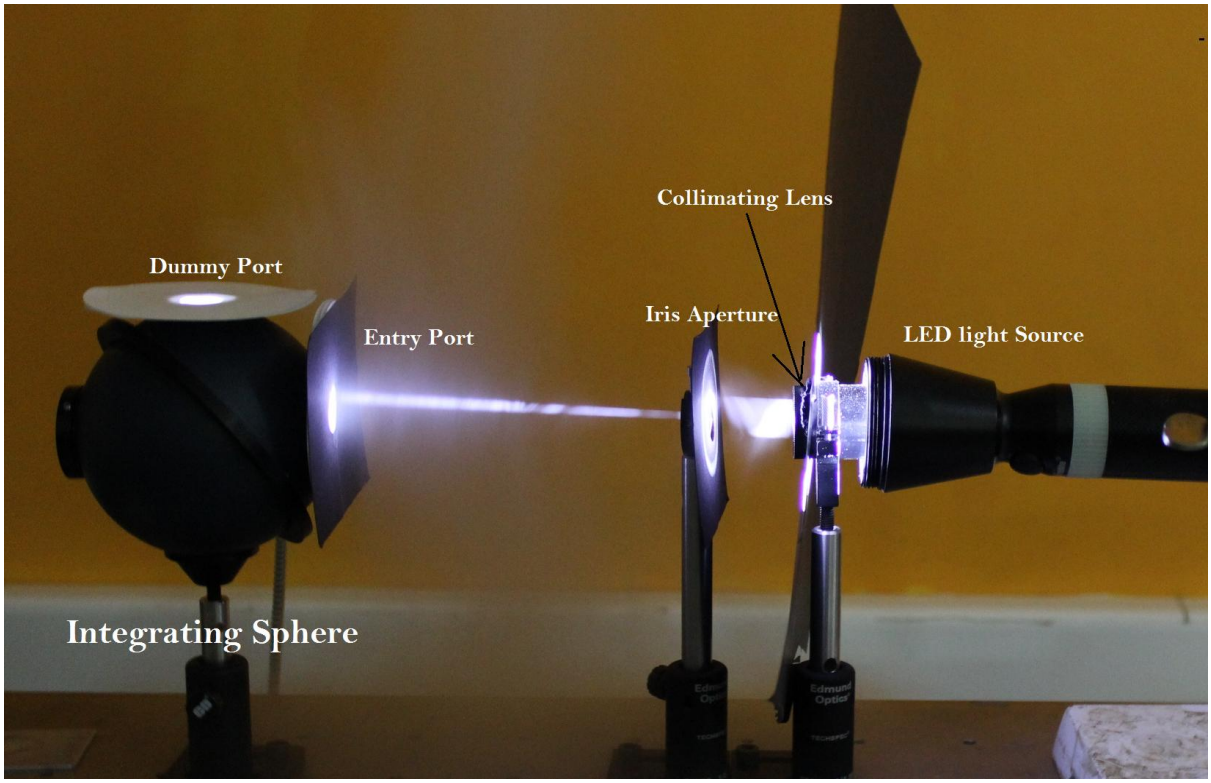

Figure 7: Custom built full spectrum transmittance system

was measured in the wavelength range of 400 nm to 650 nm with a spectral resolution of 10 nm.

To measure the wavelength transmittance, we developed an in house transmittance measurement system which is shown in Figure 7. A 1 Watt LED torch acted as the light source. The diverging beam was collimated using an achromatic lens system(Edmund Optics, USA)and the size of the light beam was regulated using an iris aperture system. A 90 mm diameter integrating sphere (Labsphere, USA) was used to collect the transmitted light. A spectrometer (ILT 900 from International light, USA) was used to analyze the collected light intensities at different wavelengths.

Chapter 4

RESULTS AND DISCUSSIONS

4.1 Empirical relations between K-M and radiative transfer coefficients

The method used to obtain the empirical relations between the radiative transfer and K-M coefficients is schematically shown in Figure 2. First, the total reflectance (*R)* and total transmittance (*T)* values of a diffusive layer were measured for various sets of μ_a and μ_s'. For a given set of *R* and *T* values, there is a unique set of *K* and *S* values which can be obtained by solving the coupled relations shown in equation 1.11. Finally, empirical relationships are obtained between the calculated sets of *K* and *S* values and the sets of radiative transfer coefficients (μ_a and μ_s') used in the samples.

4.1.1 Measurement of total reflectance and transmittance

For *R* and *T* measurements, we prepared samples with five different μ_s' values 0, 0.22, 0.41, 0.54, 0.81 and 1.63 mm^{-1} by varying the concentration of the 0.5 micron diameter microspheres, For a constant μ_s', μ_a was varied from 0 to 0.25 mm^{-1} by varying the concentration of the Premium Dark Chocolate dye shown in Figure 3. The measured total transmittance (*T*) and total reflectance (*R*) values for various values of μ_a and μ_s' at 488 nm were measured in a 750 micron cuvette and are shown in Figure 8. For increasing μ_a, both *R* and *T* decrease. With increasing μ_s', *T* decreases while *R* increases. The measured *R* and *T* values are functions of *K* and *S* as shown in equation 1.11, which in turn depend on μ_a and μ_s'.

4.1.2 Calculation of K-M coefficients *K* and *S*

Earlier authors [13-16] have shown that the K-M theory is also applicable to collimated incident beam in the regime where $\mu_s' >> \mu_a$. In the current measurement geometry, the incident beam is collimated. However, not all the samples fall in the regime $\mu_s' >> \mu_a$. Assuming that K-M theory is applicable for all ranges of μ_a and μ_s', including $\mu_a \geq \mu_s'$, the values of *K* and *S* were calculated by solving the coupled equations in equation 1.11 for various values of *R* and *T*. The calculated

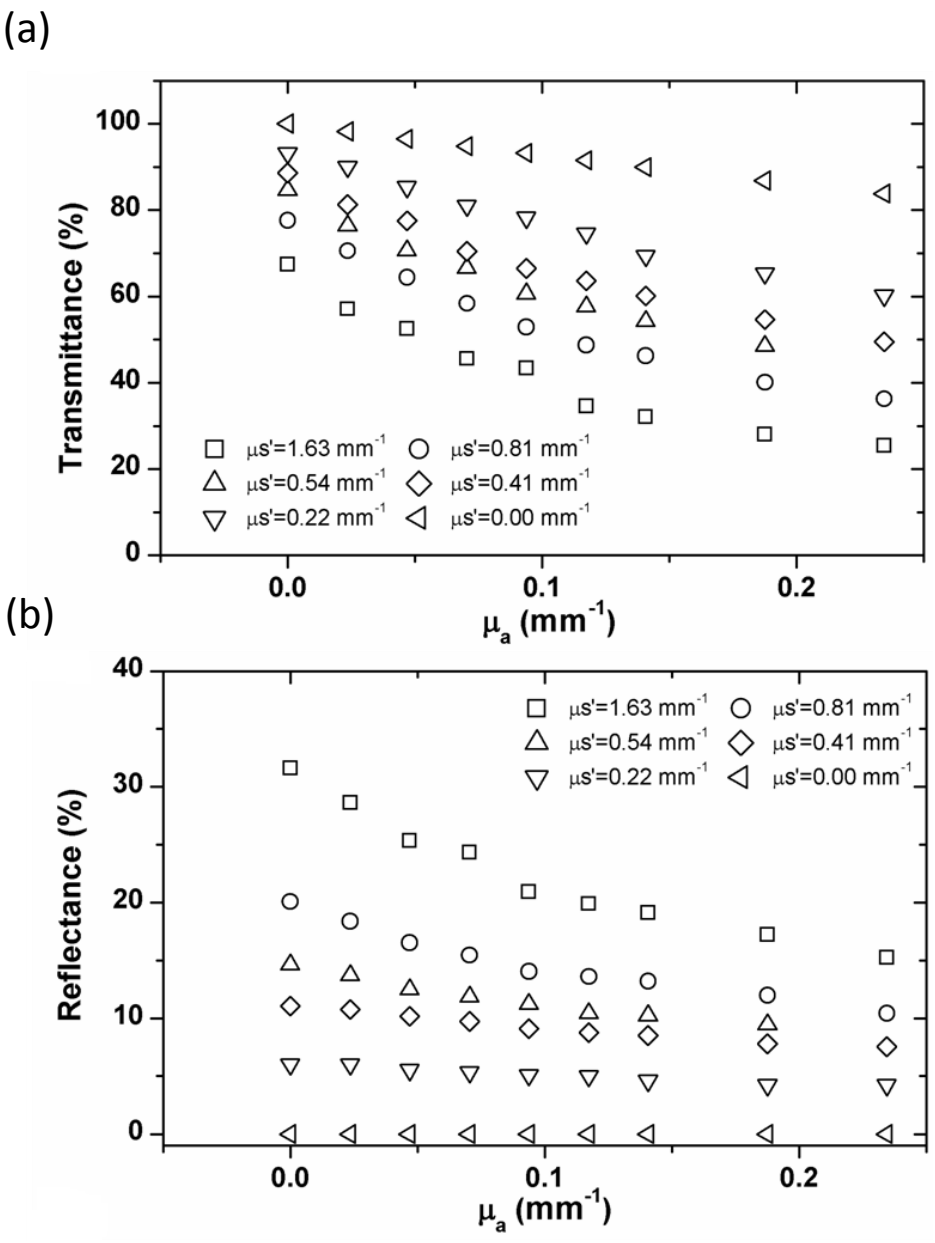

Figure 8: Measured values of total transmittance (a) and total reflectance (b) of samples for various values of μa and μs' at 488nm

*S*and *K* values are plotted as a function of μ_a for constant values of μ_s' and are shown in Figure 9a and 9b respectively. From Figure 9a, it is clear that *S* depends strongly on μ_s' and not on μ_a even in the diffusive regime $\mu_s' >> \mu_a$. Figure 9b shows the dependence of *K* as a function of μ_a and μ_s'. Unlike *S*, *K* depends on both μ_a and μ_s'. K-M absorption coefficient *K* increases as μ_a increases.

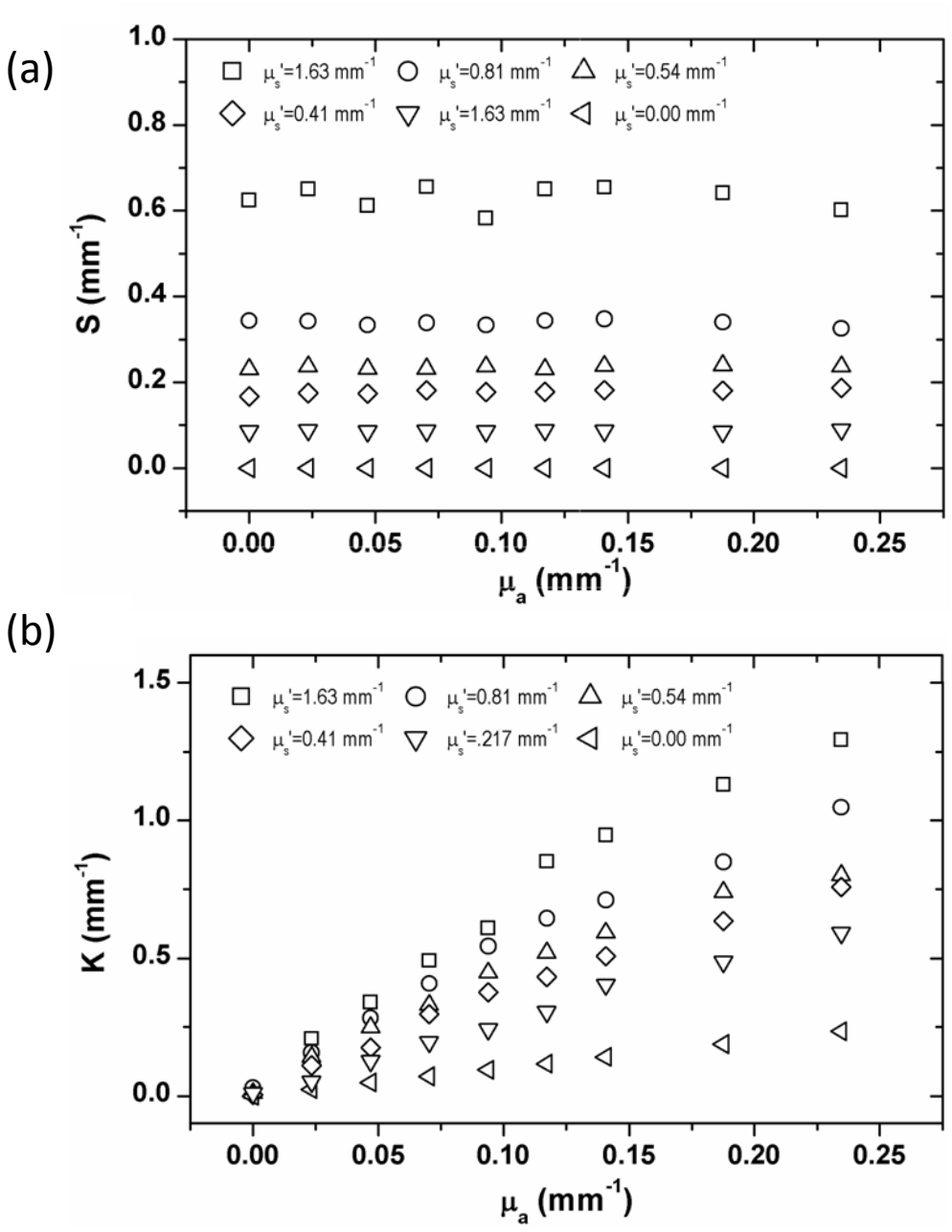

Figure 9: (a) K-M scattering coefficient *S* and (b) K-M absorption coefficient *K* for samples with various values of *μa* and *μs'*. *K* and *S* were obtained from the measured total reflectance (*R*) and total transmittance (*T*)

4.1.3 Empirical relation between K-M and Radiative transfer coefficients

From Figure 9a, it is clear that *S* depends strongly on μ_s' and not on μ_a even in the diffusive regime $\mu_s' >> \mu_a$. This is different from earlier reports which showed that the *S* depends on μ_a and μ_s' as shown in equation 2.1. Our measurement agrees with Gate's [13] and Thennadil's [16] derivation where *y* was zero. By fitting the experimental values to equation 2.1, we find the value of *x* to be 0.408.

$$S = 0.408\ \mu_s' \tag{4.1}$$

Figure 9b shows the dependence of *K* as a function of μ_a and μ_s'. Unlike *S*, *K* depends on both μ_a and μ_s'. K-M absorption coefficient *K* increases as μ_a increases. In the absence of scattering, *K* is equivalent to the absorption coefficient μ_a. Increasing μ_s' at a given μ_a further increases *K*. In the presence of scattering, *K* has an additional term which we can attribute to the absorption due to scattered photons. The absorption of the scattered photon depends not only on the absorption coefficient of the medium but also on the mean average distance travelled by the scattered photon which is proportional to its scattering coefficient [18]. A photon in a highly scattering medium will travel larger distances compared to a photon in a low-scattering medium. Hence the effective absorption of the scattered photon will depend both on the absorption coefficient and the scattering coefficient. We find that *K* follows the following empirical relation

$$K = \mu_a + a(\mu_a \mu_s')^b \tag{4.2}$$

where μ_a and μ_s' are expressed in units of mm^{-1}. By fitting our data to the above empirical relation, we find the parameter values as a=2.43 and b=0.72. We have shown in Figure 10 predicted values of *S* and *K* using the empirical relations in equation 4.1and 4.2 against values of *S* and *K* calculated from measured *R* and *T* values using equation 1.11. We see an excellent fit with R^2 values of 0.99 for both *K* and *S* implying that our empirical relation is applicable to a wide range of μ_a and μ_s'.

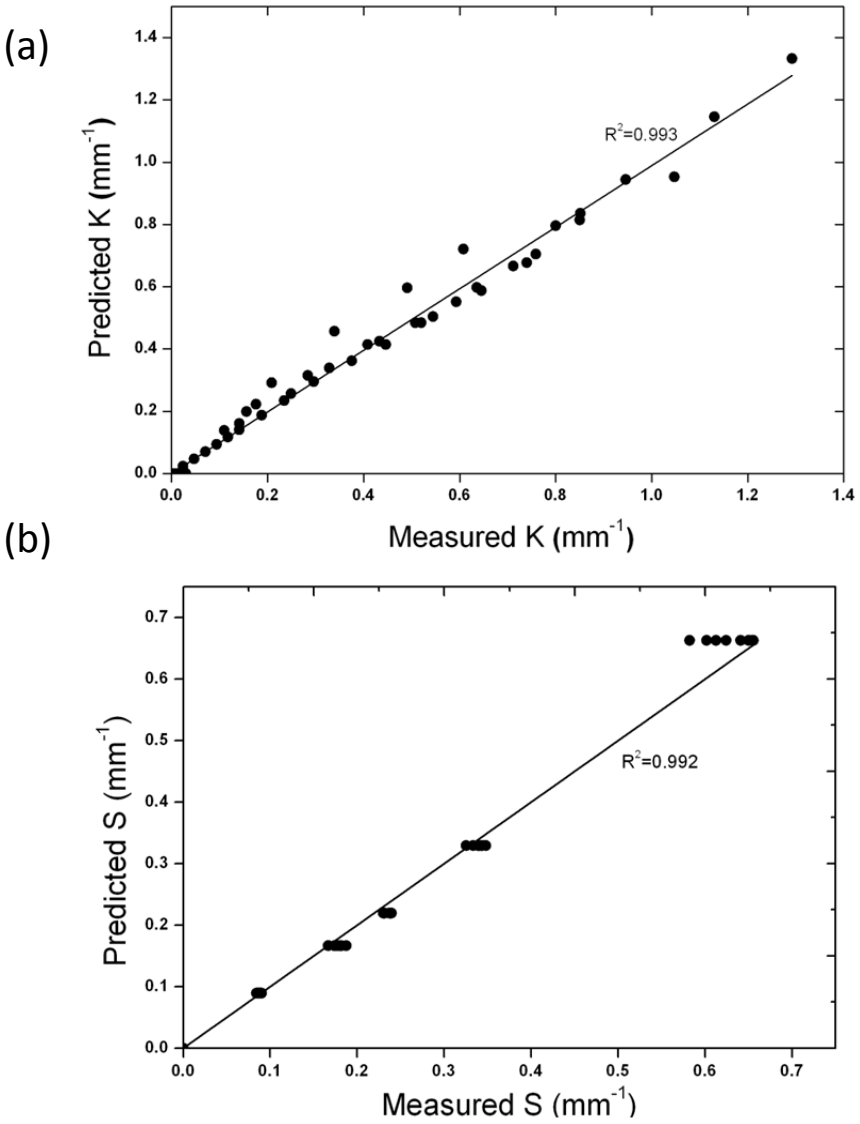

Figure 10: Predicted values of *S* and *K* using the empirical relations in Eqs. (4.1) and (4.2) as a function of *S* and *K* values calculated from measured *R* and *T* using Eq. (1.14)

4.1.4 Validation of Empirical Relations

To validate the applicability of the empirical relations in equations 4.1 and 4.2, diffusive samples were prepared using one micron polystyrene spheres and five different concentrations (0 ppm, 10 ppm, 20 ppm, 30 ppm and 40 ppm) of the Chocolate Brown TAS dye. The scattering properties of these samples were calculated using the Philip-Laven calculator [17]. Total reflectance of these diffusive samples was measured in the wavelength range of 400 to 650 nm using a commercial spectrophotometer. In this range, there is large variation of absorption as a function

of wavelength. While in certain regions $\mu_a < \mu_s'$, in other regions $\mu_a \geq \mu_s'$. Since μ_s' and μ_a of these samples are known for all the wavelengths, *K* and *S* values can be calculated using equations 4.1 and 4.2 and the reflectance for the entire wavelength range can then be predicted using equation 1.11. In Figure11a, the measured reflectance spectra (dots) of the samples with various dye concentration are shown along with the reflectance spectra predicted (solid lines) using equations 4.1 and 4.2. Good agreement was obtained between the predicted and measured reflectance spectra. The errors in the predictions are shown in Figure 11b. The maximum error in prediction was about 8% implying that the empirical relation between the optical parameters and K-M coefficient is valid over a wide range of optical parameters.

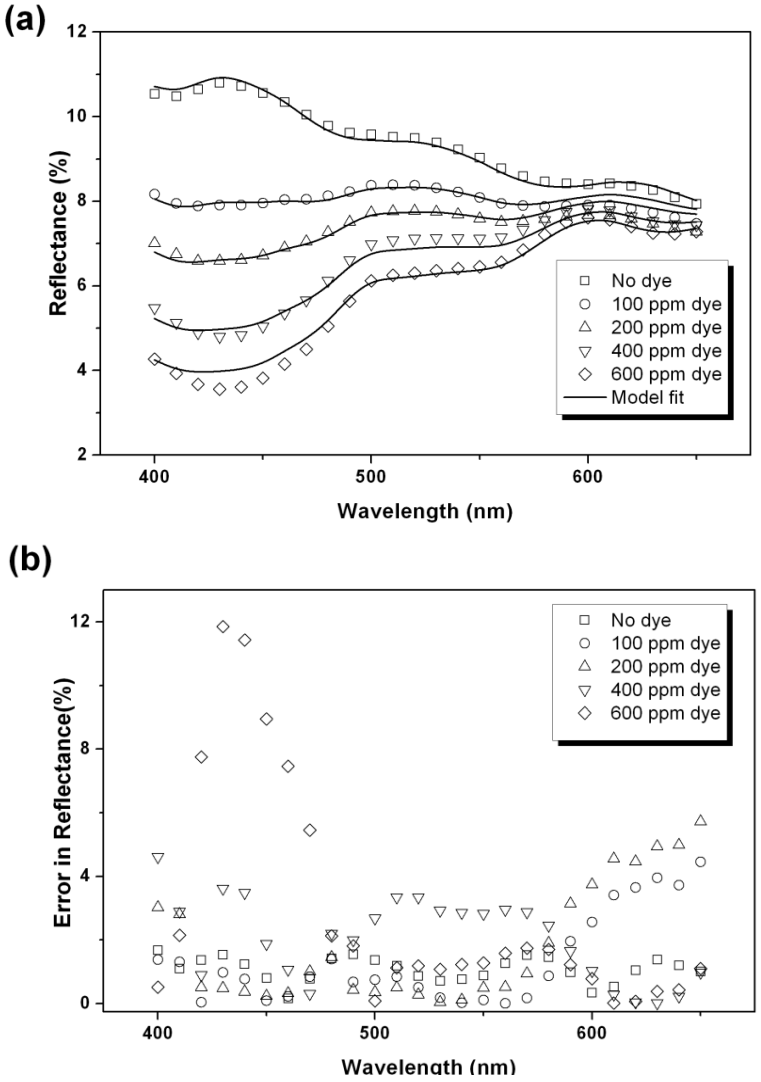

Figure 11: Measured and predicted reflectance spectra for 5 different samples (a) Reflectance values (b) Error in predicted reflectance

4.2 Applications

4.2.1 Extracting optical parameters from measured reflectance

Since the empirical relations in equations 4.1 and 4.2 are valid over wide range of optical parameters and wavelengths, it is possible to solve the inverse problem of extracting various optical parameters from the measured reflectance spectra. For example, parameters such as concentration of the chromophores and thickness of the scattering layer can be extracted simultaneously from the measured reflectance if the scattering parameters are known. This is feasible since at different wavelengths, relations in equations 4.1 and 4.2 are valid and independent of each other. One needs to solve for two unknown parameters using more than two equations.

To verify the feasibility of simultaneously extracting dye concentration and layer thickness from the measured reflectance, tissue phantoms of two different thicknesses (450 microns and 750

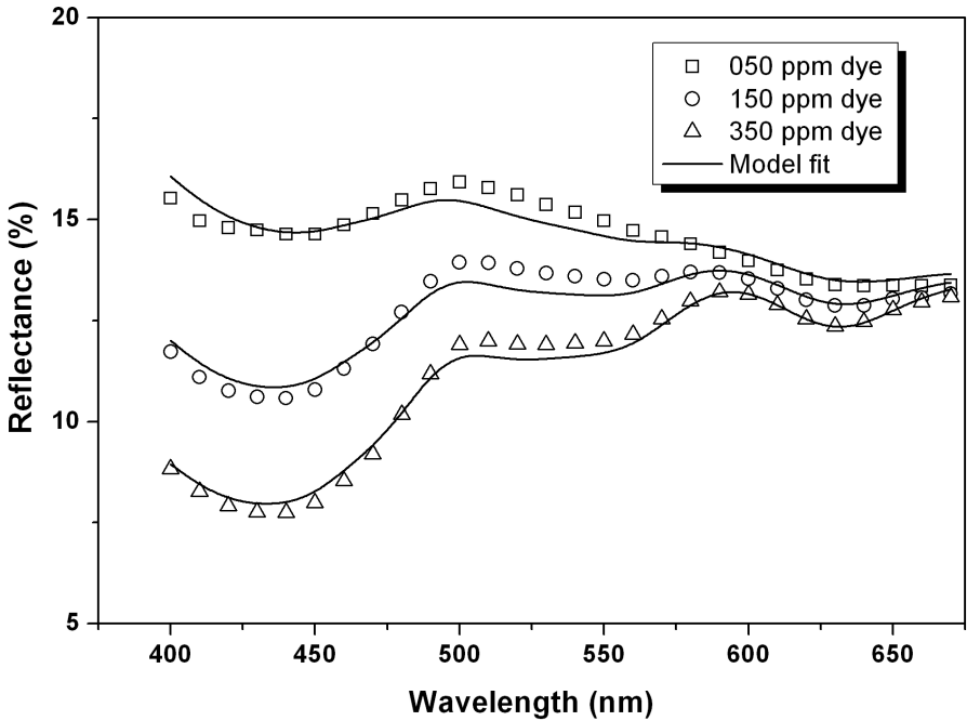

Figure 12: Solving for optical parameters from the measured reflectance spectra of tissue phantoms. The best fits were obtained by varying two fitting parameters, namely dye concentration and layer thickness. The symbols show measured reflectance, and solid lines show the best fit from the model. The actual parameter values and the predicted values are shown in Table 3

microns) were prepared using 1000 nm polystyrene spheres and different concentrations of the Chocolate Brown TAS dye. The reflectance of the tissue phantoms in the range of 400-650 nm was measured and best fit to the reflectance curves were obtained using equations 1.11, 4.1 and 4.2 by freely varying the two fitting parameters namely the concentration of the dye and thickness of the sample. The best fit obtained is shown in Figure 12 and the parameters used to obtain the best fit are shown in table 3 along with the actual parameters. While the extracted concentration values were within an error of 2-10%, the extracted thickness values were within 2% error.

Table 3 Actual and predicted values of concentration and sample thickness along with error in prediction

Concentration			Thickness		
Actual (ppm)	**Predicted (ppm)**	**Error (%)**	**Actual (ppm)**	**Predicted (ppm)**	**Error (%)**
35	32	8.6	450	444	1.3
50	49	2.0	450	455	1.1
20	18.1	9.5	750	752	0.3

4.2.2 Measurement of absorption coefficient of highly scattering particles

One of the key challenges in absorption spectroscopy is eliminating interference from scattering due to particles present in the samples. Many of the naturally occurring chromophores such as chlorophyll in leaves coexist with various scatterers. To quantify these chromophores, one needs to extract chromophores from the scattering samples through a complex extraction process. In the case of micro and nano sized inorganic particles both scattering and absorption coexist and we need a large single crystalline material to measure their absorption properties. In case of nano particles, quantum effects play a role in determining the absorption properties and are different from the bulk absorption properties. To address some of these issues, we need a method capable of decoupling absorption from scattering. We wanted to use the method that was developed here on materials which could not be studied using standard absorption spectroscopy techniques.

Colored pigments of micron and submicron sizes are heavily used in paint and cosmetic industries. Iron oxide [19] is one such pigment used in cosmetic industry. It is critical to understand the absorption and scattering properties of these materials individually in order to evaluate the benefits of the final product containing iron oxide. As an application of our methodology discussed in the earlier sections, we have used our technique to decouple the scattering and absorption of cosmetic grade iron oxide and the results are reported in this section.

Iron Oxide particles(procured from Kobo Products, USA) were dispersed in pentacyclo-siloxane oil (DC-245, Dow Corning) and stabilized using surfactants(Triethoxycaprylylsilane, Tocopherol Acetate) which do not absorb in the visible spectrum. Iron oxide particles appear red in color as shown in Figure 13 indicating that they should absorb strongly in blue and green regions.

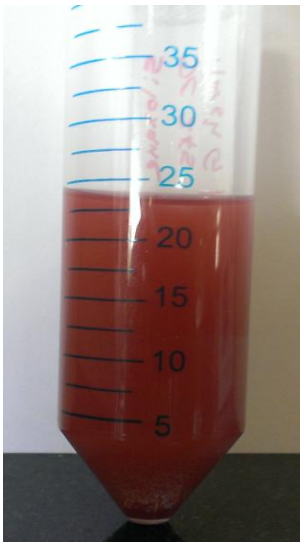

Figure 13: Iron Oxide particles dispersed in pentacyclo-siloxane oil

The absorption spectra of the iron oxide particles were measured initially using standard absorption spectroscopy techniques(UV-Vis spectrophotometer) and the spectra is shown in Figure 14 along with the absorption spectra of a standard red colored dye (Allura Red). While the absorption spectra of the dye shows a strong absorption in the blue and green region (450-600 nm), the iron oxide spectra is broad, extending into the red region also. What the UV-Vis spectrophotometer measures in the case of the iron oxide is not just the absorption but the

combined effects of scattering and absorption. This clearly shows that standard absorption spectroscopy cannot be used to measure absorption alone but can only be used to study extinction which is the combined effect of absorption and scattering.

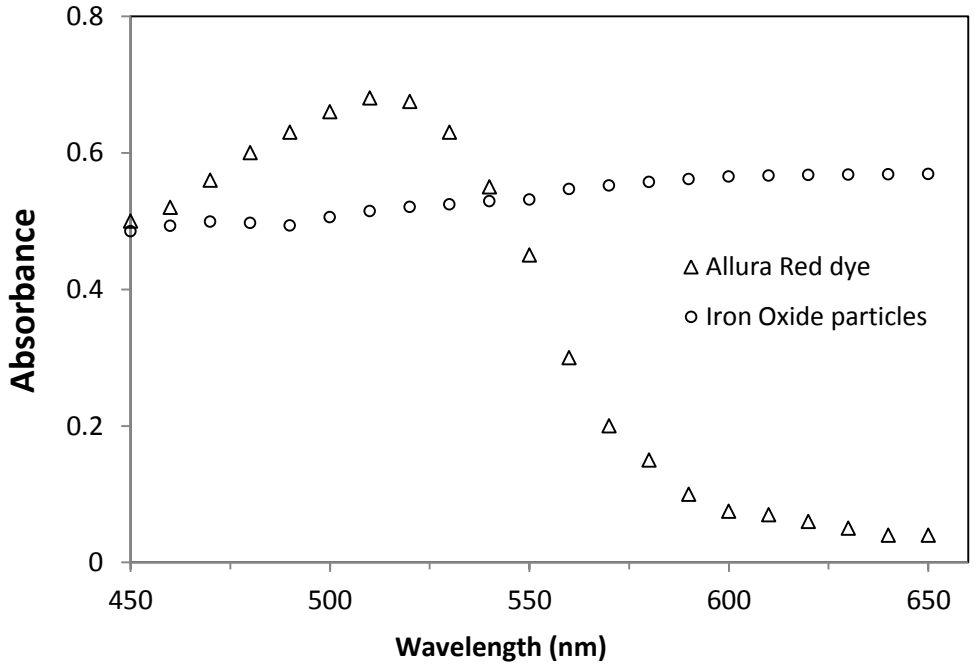

Figure 14: Measured values of absorbance of iron oxide dispersion and Allura red dye measured using a standard UV-Vis absorption spectrometer.

In order to measure the absorption of the iron oxide excluding the scattering, we prepared 4 samples of different iron oxide concentrations (0.55mg/mL, 0.87 mg/mL, 1.19 mg/mL and 1.49 mg/mL) by dispersing in pentacyclo siloxane oil. The total reflectance (*R*) and total transmittance (*T*) of the samples were measured using the integrating sphere geometry described in sections 3.2 and 3.3. The measured T and R for the four different concentrations are shown in Figure 15. The total reflectance value increases as the concentration of iron oxide increases. The reflectance values are very low in the wavelength range of 450-550 nm. The reflectance values are higher in the red region of 600-650 nm. The total transmittance value decreases as the concentration of iron oxide increases. The transmittance value is lower in the 450-550 nm range compared to the 600-650 nm range.

The T and R values were converted to K and S values using equation 1.11 and then using the empirical relationships shown in equations 4.1 and 4.2 described earlier, their μ_s' and μ_a were calculated for the wavelength range of 450-650 nm.

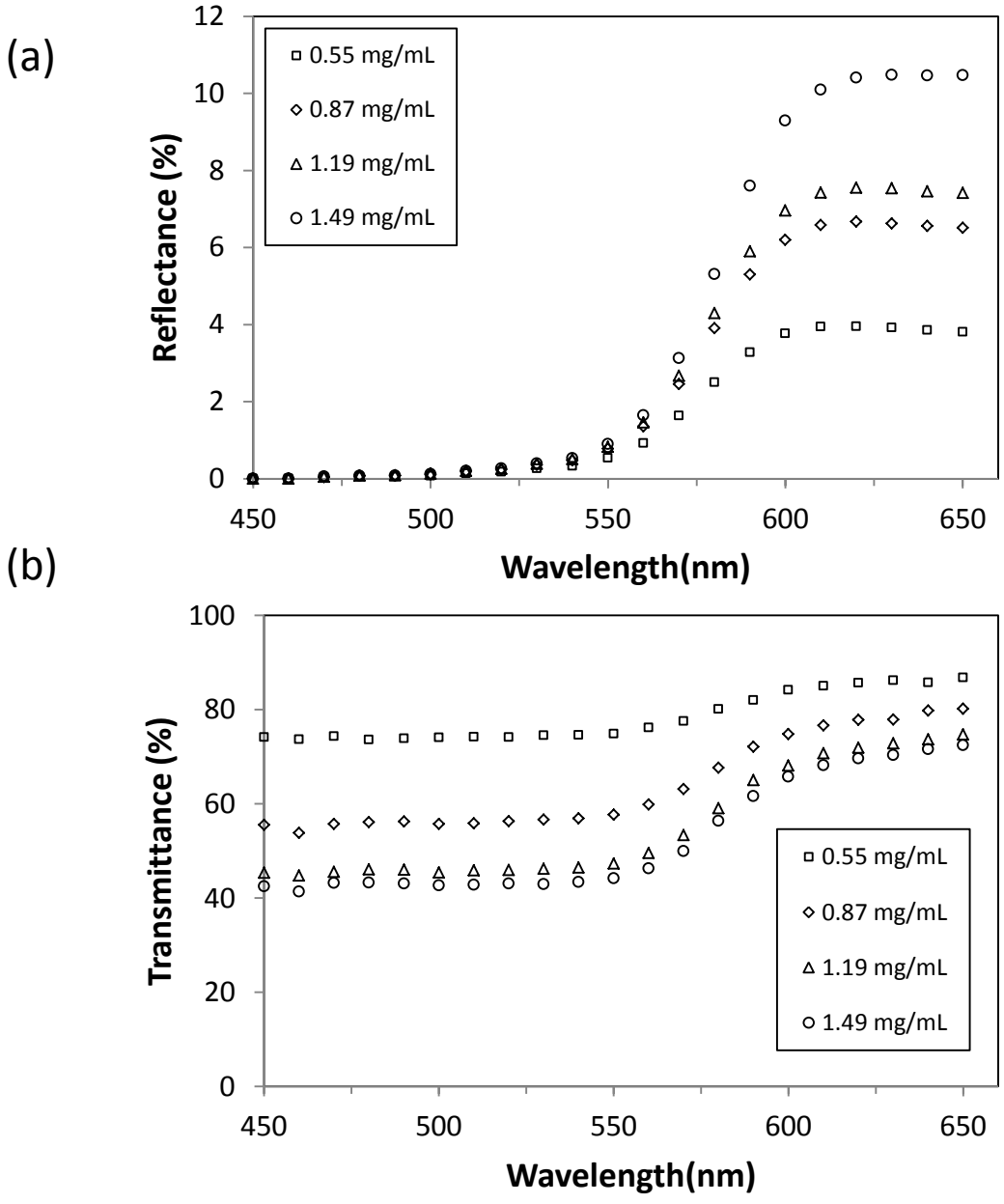

Figure 15: Measured values of (a) total reflectance R and (b) total transmittance T of 4 different concentrations of iron oxide dispersion over 450-650 nm range.

The absorption and scattering coefficients obtained this way are shown in Figure 16. From the Figure, it is evident that the iron oxide has a clear absorption in the blue-green region which is consistent with its red color. We also observe that the scattering of the iron oxide particles is low in the blue-green region and highly scattering in the red region.

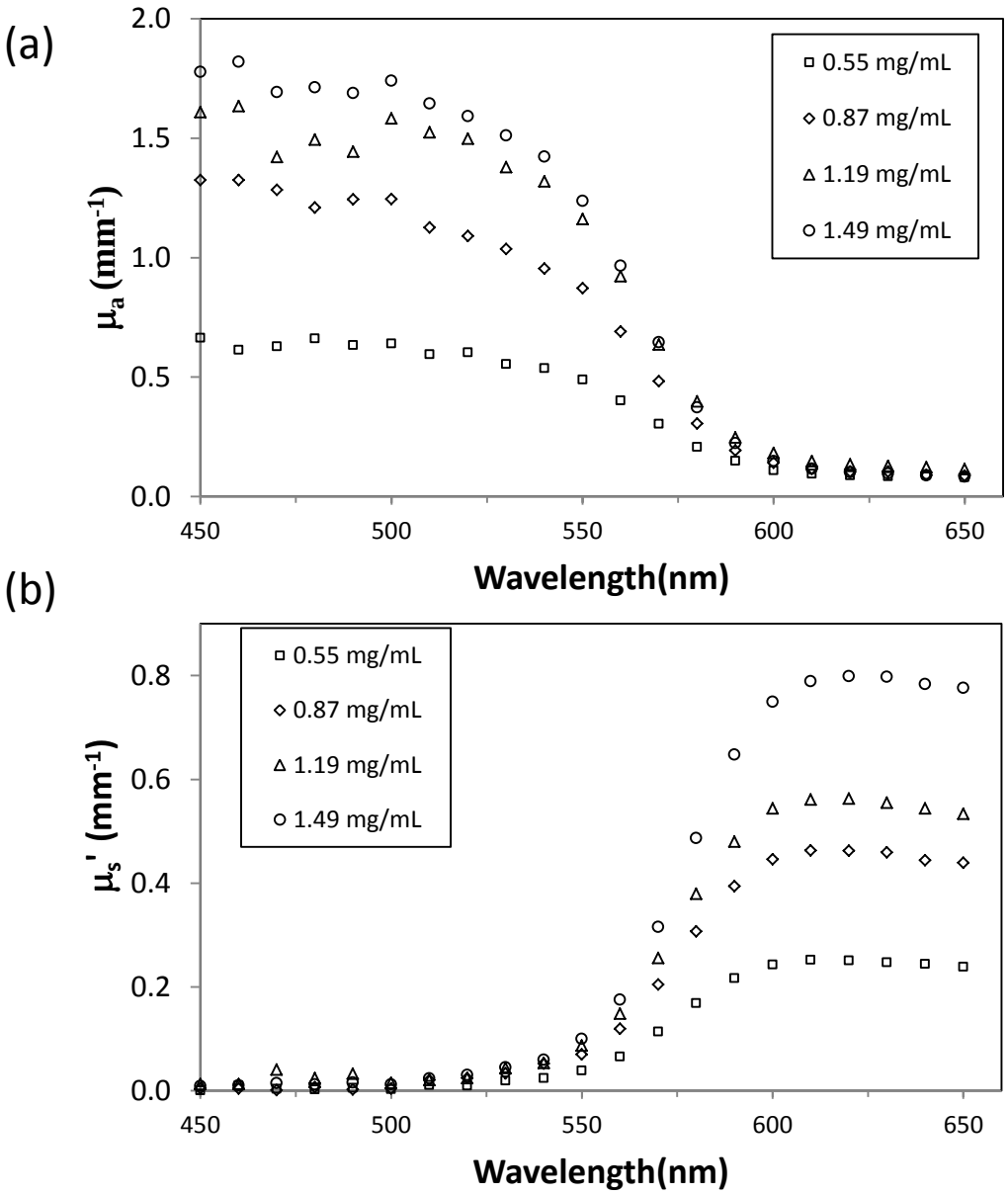

Figure 16: (a) Absorption coefficient and (b) scattering coefficient for the 4 concentrations of iron oxide dispersions. μa and μs' were obtained using equations (4.1) and (4.2) from the measured total reflectance(R) and total transmittance (T) in Figure 15

The specific absorption coefficient of the media is defined as the absorption coefficient per unit concentration. It is independent of the concentration. We have calculated the average of the specific absorption coefficient of the four samples and shown in Figure 17.

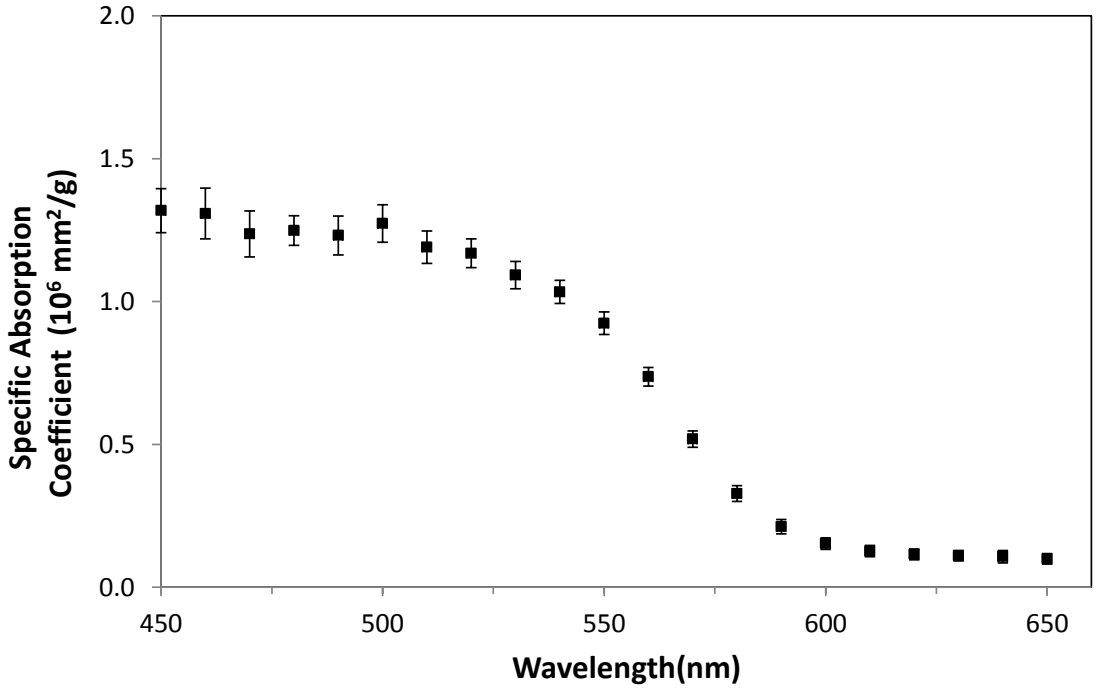

Figure 17: Specific Absorption coefficient of iron oxide particles. Error bars indicate standard deviation of four different concentrations.

It is evident that our method is capable of measuring the specific absorption coefficient of iron oxide within a 5-10% error. Further our method is capable of decoupling the specific absorption and scattering coefficients, irrespective of the concentrations used, within an error range of 5-10%

Chapter 5

CONCLUSION

One of the key challenges in strongly scattering media is to decouple absorption from scattering. Various authors have tried to use diffuse optical spectroscopy to address this. However, these measurements involve computer intensive calculations to obtain optical parameters from the diffuse optical spectra. To address this, in this thesis, we wanted to obtain a simple empirical relation which can relate the optical parameters to the measured diffuse reflectance and transmittance spectra.

We have developed an integrating sphere based diffuse optical measurement system. Using the system, we measured total transmittance and total reflectance of samples with varying optical parameters and obtained empirical relations between K-M coefficients and the radiative transport coefficients which are valid both in the diffusive and non-diffusive regimes. Our empirical relations show that the K-M scattering coefficients depend only on reduced scattering coefficient (μ_s') while the K-M absorption coefficient depends both on absorption (μ_a) and reduced scattering (μ_s') coefficients of radiative transfer theory. We have shown that these empirical relations can predict total reflectance within an error of 10%. They also can be used to solve the inverse problem of obtaining multiple optical parameters such as chromophores concentration and sample thickness from the measured reflectance spectra with a maximum accuracy of 90-95%.

We have also used our method to decouple the absorption and scattering properties of micron sized iron oxide particles which is not possible with standard absorption spectroscopy techniques. Our method is capable of measuring the specific absorption of iron oxide within 5-10% error. This method along with the derived empirical relations can be further extended to UV regimes to study nanoparticles which are of relevance in various photonic applications.

REFERENCES

1. Pierre Bouguer, Essai d'Optique, sur la gradation de la lumiere ,Claude Jombert, pp. 16–22, 1729
2. August Beer, Determination of the absorption of red light in colored liquids, Annalen der Physik und Chemie, vol. 86, pp. 78–88, 1852
3. Lord Rayleigh ,On the scattering of light by small particles, Philosophical Magazine, series 4, vol. 41, 447-454, 1871
4. Mirozlaw Jonasz , Scattering coefficients (www.tpdsci.com/Tpc/ScaCf.php), 2006
5. Jenni Heino, Anisotropic effects in highly scattering media, Physical Review E 68, 031908 , 2003
6. C.F. Bohren, Multiple scattering of light and some of its observable consequences, American Journal of Physics, Vol 55(6), 524–533, 1987
7. A. Ishimaru, Wave Propagation and Scattering in Random Media, Vol. 1, Academic Press, New York,1978
8. K. M. Case and P. F. Zweifel, Linear Transport Theory Addison- Wesley, Reading, PA , 1967
9. P. Kubelka and F. Munk, Ein Beitrag zur Optik der Farbanstriche, Zeits. f. tech. Physik 12, 593–601, 1931
10. K. Klier, Absorption and scattering in plane parallel turbid media, J. Opt. Soc. Am. 62(7), 882–885,1972
11. M. J. C. van Gemert and W. M. Star,Relations between the Kubelka–Munk and transport equation models for anisotropic scattering, Lasers Life Sci. 1, 287–298, 1987
12. B. J. Brinkworth, Interpretation of the Kubelka–Munk coefficients in reflection theory, Appl. Opt. 11(6), 1434–1435, 1972
13. L. F. Gate, Comparison of the photon diffusion model and Kubelka–Munk equation with the exact solution of the radiative transport equation, Appl. Opt. 13(2), 236–238, 1974
14. J. T. Atkins, Absorption and scattering of light in turbid media, Ph.D. Dissertation, University of Delaware, 1965
15. J. Reichman, Determination of absorption and scattering coefficients for non-homogeneous media, Appl. Opt. 12(8), 1811–1815, 1973
16. S. N. Thennadil, Relationship between the Kubelka–Munk scattering and radiative transfer coefficients, J. Opt. Soc. Amer. A. 25(7),1480–1485,2008

17. Philip Laven, “A computer program for scattering of light from a sphere using Mie theory & the Debye series,” http://www.philiplaven.com/ mieplot.htm (October 24, 2012).

18. R. Reif, O. A’Amar, and I. J. Bigio, Analytical model of light reflectance for extraction of the optical properties in small volumes of turbidmedia, Appl. Opt.46(29), 7317–7318, 2007

19. H Pardoe , Structural and magnetic properties of nanoscale iron oxide particles synthesized in the presence of dextran or polyvinyl alcohol, Journal of Magnetism and Magnetic Materials, Vol. 225, Issue 1-2, 41-46, 2001

APPENDIX

A portion of the results described above have been published in the November 2012 issue of the **Journal of Bio-Medical Optics** titled "*Empirical relationship between Kubelka–Munk and radiative transfer coefficients for extracting optical parameters of tissues in diffusive and nondiffusive regimes*"; authored by Arindam Roy, Rajagopal Ramasubramaniam and Harshavardhan A. Gaonkar

http://dx.doi.org/10.1117/1.JBO.17.11.115006

Journal of Biomedical Optics 17(11), 115006 (November 2012)

Empirical relationship between Kubelka–Munk and radiative transfer coefficients for extracting optical parameters of tissues in diffusive and nondiffusive regimes

Arindam Roy,[a] Rajagopal Ramasubramaniam,[a] and Harshavardhan A. Gaonkar[b]
[a]Unilever R&D Bangalore, 64 Main Road, Whitefield, Bangalore, 560066, India
[b]Indian Institute of Science Education and Research, Dr. Homi Bhabha Road, Pune, 411008, India

Abstract. Kubelka–Munk (K-M) theory is a phenomenological light transport theory that provides analytical expressions for reflectance and transmittance of diffusive substrates such as tissues. Many authors have derived relations between coefficients of K-M theory and that of the more fundamental radiative transfer equations. These relations are valid only in diffusive light transport regime where scattering dominates over absorption. They also fail near boundaries where incident beams are not diffusive. By measuring total transmittance and total reflectance of tissue phantoms with varying optical parameters, we have obtained empirical relations between K-M coefficients and the radiative transport coefficients for integrating sphere-based spectrophotometers that use uniform, nondiffusive incident beams. Our empirical relations show that the K-M scattering coefficients depend only on reduced scattering coefficient (μ_s'), whereas the K-M absorption coefficient depends on both absorption (μ_a) and reduced scattering (μ_s') coefficients of radiative transfer theory. We have shown that these empirical relations are valid in both the diffusive and nondiffusive regimes and can predict total reflectance within an error of 10%. They also can be used to solve the inverse problem of obtaining multiple optical parameters such as chromophore concentration and tissue thickness from the measured reflectance spectra with a maximum accuracy of 90% to 95%. [DOI: 10.1117/1.JBO.17.11.115006]

Keywords: absorption; diffuse reflectance; Kubelka-Munk; radiative transfer; scattering; tissue optics; tissues thickness.

Paper 12470 received Jul. 21, 2012; revised manuscript received Oct. 15, 2012; accepted for publication Oct. 18, 2012; published online Nov. 8, 2012.